JMEPEG (2009) 18:319–323
DOI: 10.1007/s11665-008-9282-9

1059-9495/$19.00

Corrosion and Stress Corrosion Cracking Behavior of X70 Pipeline Steel in a CO_2-Containing Solution

L. Zhang, X.G. Li, C.W. Du, and Y.F. Cheng

(Submitted April 9, 2008; in revised form July 3, 2008)

The electrochemical corrosion and stress corrosion cracking (SCC) behaviors of X70 pipeline steel in CO_2-containing solution were studied by electrochemical measurements, slow strain rate tensile tests, and surface characterization. The results found that the electrochemical corrosion of X70 steel in aerated, alkaline solution is an activation-controlled process, and a stable passivity cannot develop on steel. Corrosion rate of the steel increases with the CO_2 partial pressure. The enhanced anodic dissolution due to the additional cathodic reaction in the presence of CO_2, rather than the film-formation reaction, dominates the corrosion process. The mass-transfer step through $FeCO_3$ deposit is the rate-controlling step in corrosion of the steel. The susceptibility of steel to SCC and the fracture brittleness increase with the CO_2 partial pressure. The enhanced fracture brittleness is attributed to the evolution and penetration of hydrogen atoms into the steel, contributing to crack propagation. The formed deposit layer is not effective in reducing hydrogen permeation due to the loose, porous structure.

Keywords CO_2, corrosion, pipeline steel, stress corrosion cracking

1. Introduction

The enhanced corrosion of pipeline steels under the condition where CO_2 is present has been a serious problem in the oil and gas industry. It has been acknowledged (Ref 1) that carbon dioxide accelerates the rates of general corrosion and localized corrosion of carbon steel, sometimes as pitting corrosion. Theories and models have been developed to illustrate CO_2 corrosion of steel (Ref 1-3). These variously involve interaction of CO_2 with both anodic reaction and cathodic reaction. Moreover, since CO_2 is associated with water to give carbonic acid, and then dissociates into bicarbonate and carbonate anions, the mechanisms have also involved interactions at the acidic pH (Ref 4). Furthermore, the effect of CO_2 partial pressure on corrosion of steel has been considered (Ref 5, 6), and the corrosion rate increases as CO_2 solubility increases with the increasing CO_2 partial pressure.

Stress corrosion cracking (SCC) has been recognized as one essential threat to integrity of pipelines (Ref 7). To date, extensive work has been performed to investigate pipeline SCC (Ref 7-10). For example, two types of SCC, i.e., high pH SCC and near-neutral pH SCC, have been found to occur on pipelines, and the associated environmental conditions have been identified. While the former occurs under a concentrated carbonate-bicarbonate solution, the latter is always associated with a dilute bicarbonate solution where $5\%CO_2/95\%N_2$ is purged to keep the near-neutral solution pH. With the further increase of CO_2 partial pressure, it is expected that the solution pH continues to decrease. The steel will experience different corrosion and SCC behavior from those under near-neutral pH conditions. To date, there has been limited research conducted on the corrosion and SCC of pipelines in the presence of significant amounts of CO_2, and thus, the acidic pH condition.

In this work, electrochemical corrosion behavior and SCC susceptibility of X-70 pipeline steel were investigated by various electrochemical measurements, including potentiodynamic polarization curves and electrochemical impedance spectroscopy (EIS), slow strain rate tensile (SSRT) tests and surface characterization techniques. The effect of CO_2 partial pressure was determined and the corrosion mechanism was analyzed. It is anticipated that this research develops an essential correlation between corrosion and SCC behavior of pipelines in the presence of significant amounts of CO_2.

2. Experimental

2.1 Electrode and Solution

Test electrodes were made from X70 steel sheet with the chemical composition listed in Table 1. The mechanical properties of the steel measured at room temperature were provided by supplier shown as follows: tensile strength equal to 675 MPa; yield strength equal to 592 MPa; and elongation to failure equal to 26%. The specimens were embedded in epoxy resin leaving a working area of 1 cm^2. The electrode preparation was carefully controlled to ensure that there was no bubble at the epoxy/steel interface. The working surface of electrode was subsequently polished with 800 grit and 1000 grit emery papers, cleaned by distilled water and methanol.

L. Zhang, X.G. Li, and **C.W. Du**, School of Materials Science and Engineering, University of Science and Technology Beijing, Beijing 100083, China; and **Y.F. Cheng**, Department of Mechanical and Manufacturing Engineering, University of Calgary, Calgary, AB, Canada T2N 1N4. Contact e-mail: lixiaogang99@263.net.

The test solution was a soil-extracted solution, with the chemical composition shown in Table 2, purged with different amount of CO_2, i.e., 0, 5, 10, 15, 20, 100% CO_2 balanced with high purity N_2 gas for 2 h prior to and throughout the tests.

All the tests were performed at ambient temperature.

2.2 Electrochemical Measurements

Electrochemical measurements, including potentiodynamic polarization curves and EIS, were performed in a three-electrode cell using an EG&G Model 273A potentiostat. X70 pipe steel electrode was used as working electrode, a platinum wire as counter electrode and a saturated calomel electrode (SCE) as reference electrode. During polarization curve measurements, the potential scan rate was 0.5 mV/s. The ohmic potential drop was compensated by the instrument. During EIS measurements, an AC disturbance signal of 10 mV was applied on the electrode at open-circuit potential. The measuring frequency ranged from 0.01 to 100000 Hz.

2.3 SSRT Tests

The SSRT tests were performed in air and in the solution at a strain rate of 1×10^{-6} s^{-1}. A typical plate tensile specimen was designed based on GB T15970 (Fig. 1) and was used for SSRT tests. After failure, the fracture surface of the specimen was examined by scanning electron microscopy (SEM). The susceptibility to SCC was described by the percentage of reduction-in-area (ψ%):

$$\psi(\%) = \frac{(S_i - S_f) \times 100}{S_i} \quad \text{(Eq 1)}$$

where S_f and S_i were the cross-section areas of the tensile specimen after and before test, respectively.

Table 1 Chemical composition of X70 pipeline steel

Elements	C	Si	Mn	P	S	V	Ti	Nb	Fe
Weight, %	0.055	0.22	1.62	0.013	0.002	0.030	0.009	0.070	Balance

Table 2 Chemical composition (g/L) of the test solution

$CaCl_2$	NaCl	Na_2SO_4	$MgCl_2{\cdot}6H_2O$	$NaHCO_3$
0.2442	3.1707	2.5276	0.3135	0.1462

3. Results

3.1 Electrochemical Tests

Figure 2 shows the polarization curves of X70 steel in the solutions with different amounts of CO_2. The fitted electrochemical parameters, including polarization resistance (R_p) and corrosion current density (i_{corr}), and solution pH are listed in Table 3. It is seen that, with the increasing CO_2 content, the solution pH decreased and corrosion current density increased. Furthermore, the anodic polarization behavior did not show a passive region in the absence of CO_2 even in an aerated, alkaline environment.

Figure 3 shows the Nyquist diagrams of X70 steel in the absence and presence of CO_2. It is seen that there were two time constants in the frequency range in the presence of CO_2,

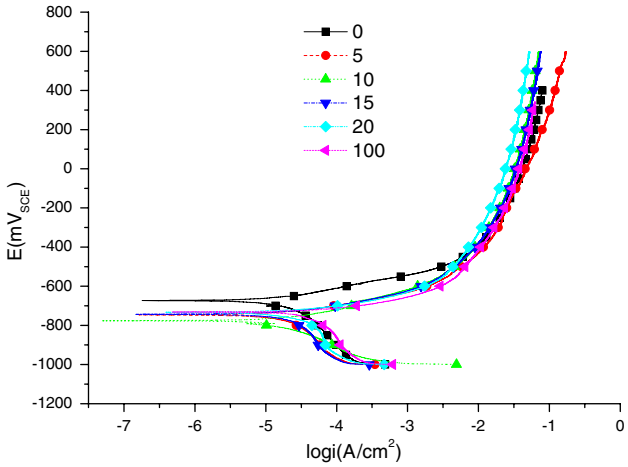

Fig. 2 Polarization curves of X70 steel in the solution with different CO_2 partial pressures

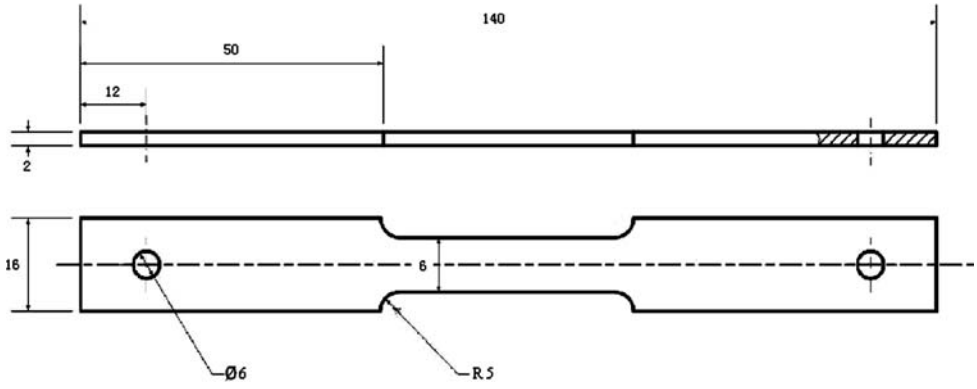

Fig. 1 Schematic diagram of the tensile specimen

Table 3 Electrochemical parameters fitted from the polarization curves

CO_2, %	0	5	10	15	20	100
R_p, Ω	1371	1045	1203	881.1	629.5	292.5
I_{corr}, μA/cm^2	11.51	20.78	21.94	24.64	34.49	74.23
pH	8.90	5.73	5.55	5.46	5.29	5.05

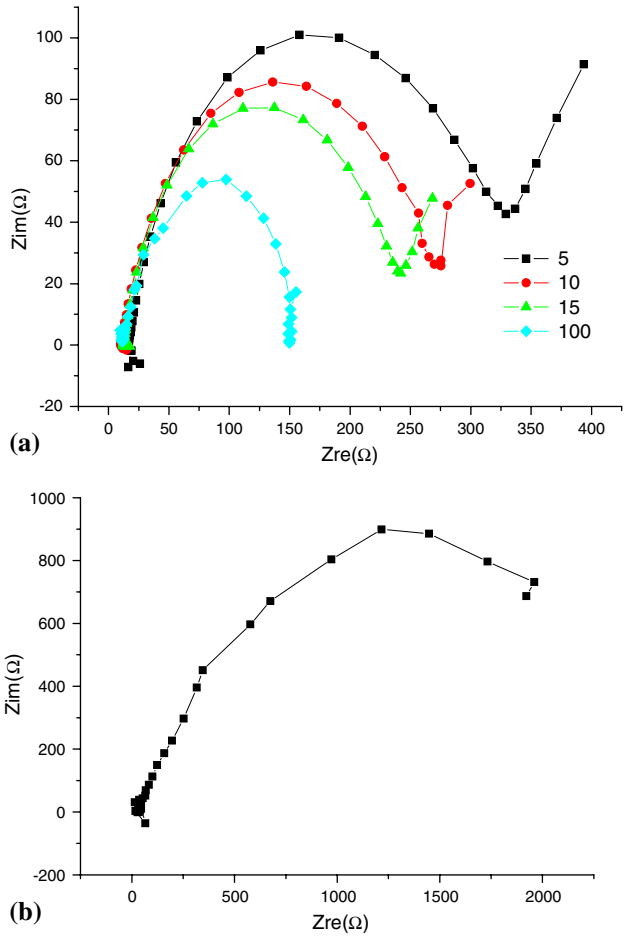

Fig. 3 Nyquist diagrams of X70 steel in the presence of CO_2 (a) and in the absence of CO_2 (b)

that is, a semicircle in the high-frequency range and a Warburg diffusive impedance in the low-frequency range (Fig. 3a). The size of the high-frequency semicircle decreased with the increase of CO_2 in the solution. In the absence of CO_2, the impedance plot was dominated with one time constant only, i.e., a semicircle over the whole frequency range (Fig. 3b).

3.2 Slow Strain Rate Test

Figure 4 shows the stress-strain curves of X70 steel in the solution with different CO_2 partial pressures. The calculated susceptibility of steel to SCC is shown in Fig. 5. It is seen that there was a rapid drop of reduction-in-area, i.e., a rapid increase of SCC susceptibility, when the solution was purged with CO_2. Furthermore, with the increase of CO_2 partial pressure, the susceptibility of steel to SCC continued to increase until a relatively steady value was reached at about 20% CO_2.

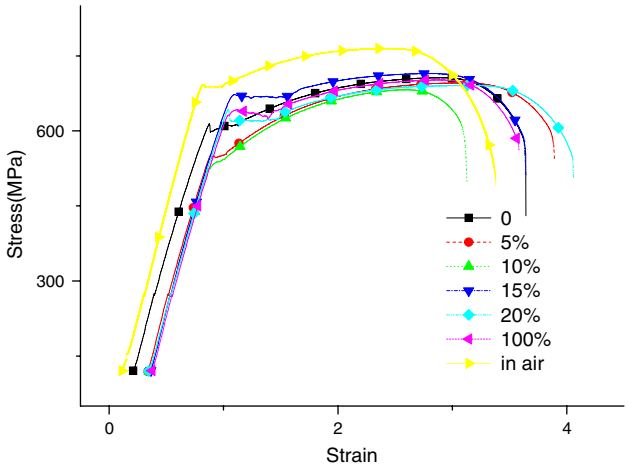

Fig. 4 Stress-strain curves of X70 steel in the solutions with different CO_2 partial pressures

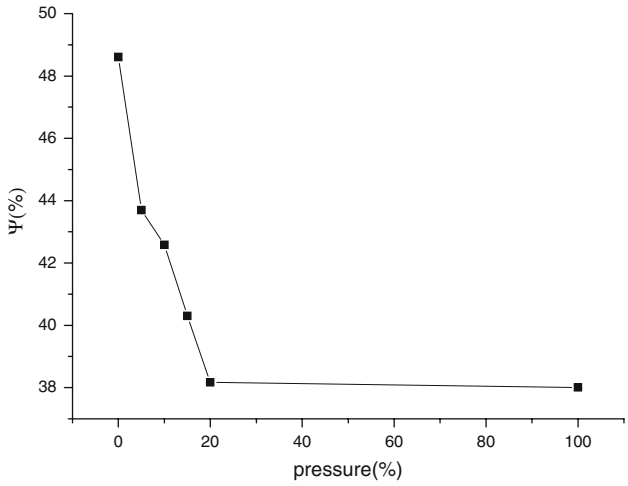

Fig. 5 Effect of CO_2 partial pressure e on percentage of reduction-in-area

3.3 Fractographic Observation

Figure 6 shows the SEM views of fracture surface morphologies of X70 steel after SSRT tests. It is seen that the fracture surface tested in air was dominated by ductile fracture features, with extensive distribution of dimples (Fig. 6(a)). The surface morphologies of the specimens tested in 5% and 10% were characterized with a mixed ductile-brittle feature (Fig. 6 (b) and (c)). With the further increase of CO_2 partial pressure, the fracture surfaces showed signs of brittle fracture, with increasing signs of cleavage, as shown in Fig. 6 (d), (e), and (f).

4. Discussion

In the alkaline, aerated solution, the cathodic reaction is dominated by oxygen reduction:

$$O_2 + 2H_2O + 4e \rightarrow 4OH^- \quad \text{(Eq 2)}$$

The anodic process is described as a multiple-step oxidation reaction of iron (Ref 11, 12), with the formation $Fe(OH)_2$

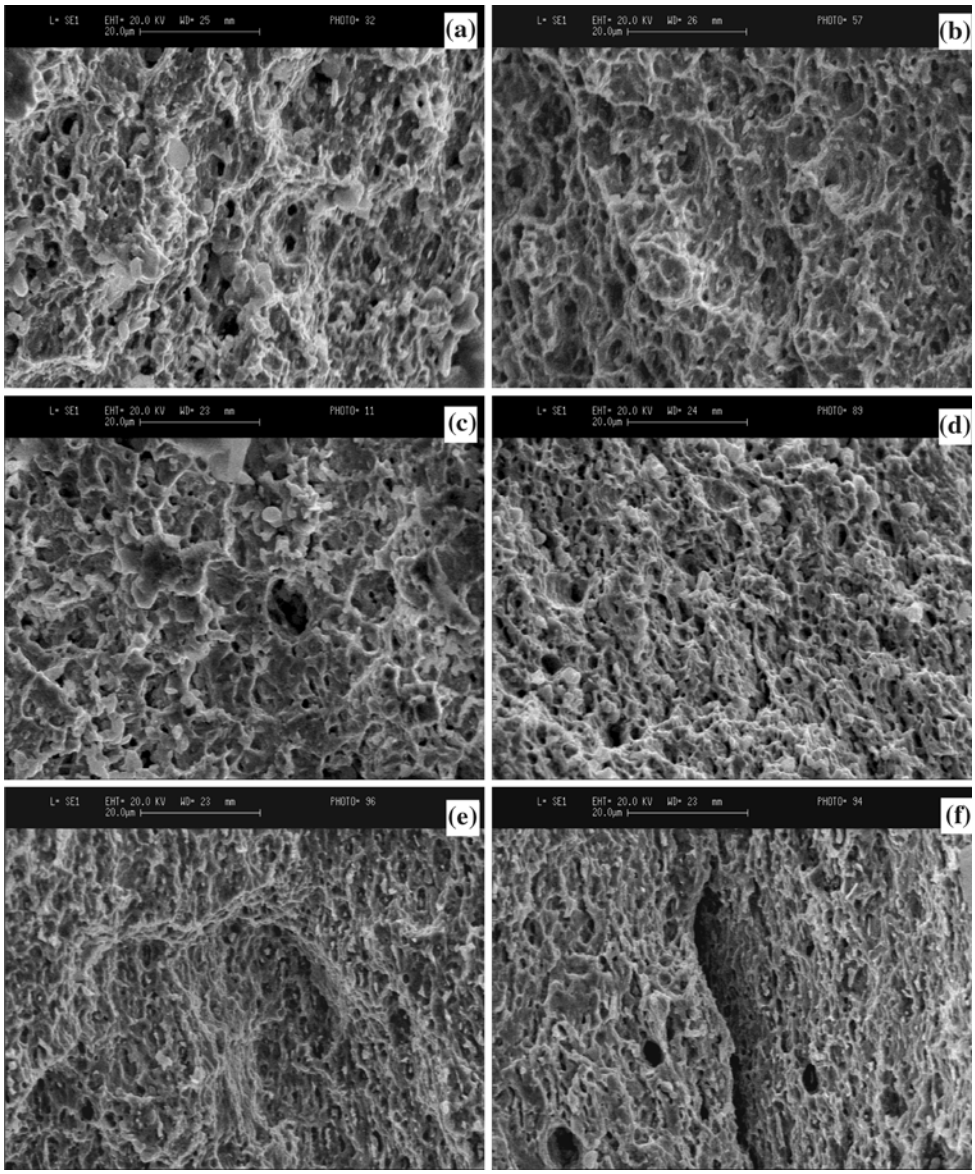

Fig. 6 SEM morphologies of X70 steel fracture surface at the different CO_2 partial pressures (a) 0%, (b) 5%, (c) 10%, (d) 15%, (e) 20%, and (f) 100%

$$Fe + H_2O \rightarrow Fe(OH) + H^+ + e \quad \text{(Eq 3)}$$

$$Fe(OH) \rightarrow Fe(OH)^+ + e \quad \text{(Eq 4)}$$

$$Fe(OH)^+ + OH^- \rightarrow Fe(OH)_2 \rightarrow \text{hydrous } Fe(OH)_2 \text{layer} \quad \text{(Eq 5)}$$

The $Fe(OH)_2$ layer could block corrosive species approaching the electrode surface to inhibit the further corrosion of steel. However, it is a stable passive film. The present work (Fig. 2) shows that a stable passive region could not be developed on steel, and characterized by one time constant, i.e., one semicircle over the measured frequency range. The impedance plot indicates an activation-controlled corrosion process.

In the presence of CO_2, the dissolved CO_2 is hydrated to form the weak acid, H_2CO_3, by

$$CO_2 + H_2O \rightarrow H_2CO_3 \quad \text{(Eq 6)}$$

The H_2CO_3 then dissociates by a two step process, resulting in the decrease of solution pH:

$$H_2CO_3 \rightarrow H^+ + HCO_3^- \quad \text{(Eq 7)}$$

$$HCO_3^- \rightarrow H^+ + CO_3^{2-} \quad \text{(Eq 8)}$$

At pH < 4, the reduction of hydrogen ions is the dominant cathodic reaction. At pH between 4 and 6, in addition to the reduction of hydrogen ions, a new cathodic reaction becomes important:

$$H_2CO_3 + e \rightarrow H + HCO_3^- \quad \text{(Eq 9)}$$

This additional cathodic reaction is the main reason for the higher corrosion rate of the steel in CO_2 (Ref 13). The present

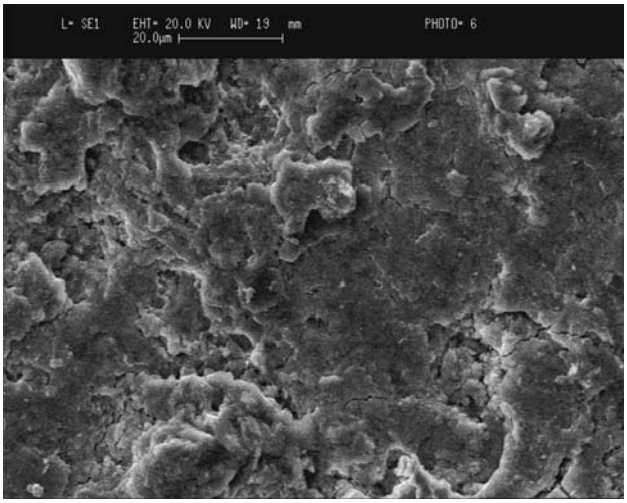

Fig. 7 SEM view of corrosion product formed on the steel surface in CO_2-containing solution

work (Fig. 2 and Table 3) shows that the corrosion current density of steel increases with the increasing CO_2 partial pressure, which is associated with the enhanced acidity of the solution.

During corrosion of the steel in CO_2, when the concentrations of Fe^{2+} and CO_3^{2-} ions exceed the solubility limit, the solid iron carbonate film will form and deposit on the steel surface:

$$Fe^{2+} + CO_3^{2-} \Rightarrow FeCO_3 \quad \text{(Eq 10)}$$

$$Fe(OH)_2 + CO_2 \rightarrow FeCO_3 + H_2O \quad \text{(Eq 11)}$$

It has been reported (Ref 14) that the formation of iron carbonate film would inhibit the corrosion of steel. However, this work did not find this to occur. Actually, the complexity of CO_2 corrosion of the steel comes from the competition between the enhanced anodic dissolution due to the additional cathodic reaction (9) and the film-formation reaction (10). The present work indicates that the enhanced anodic dissolution dominates the whole corrosion process. Furthermore, the impedance measurements show a diffusive impedance in the low-frequency range, indicating that mass-transfer through $FeCO_3$ becomes the rate-controlling step. The surface morphology of the deposit layer is shown in Fig. 7.

The present work shows that the SCC susceptibility of the steel increases with the CO_2 partial pressure, as shown in Fig. 4 and 5. Furthermore, the fracture brittleness is enhanced by the presence of CO_2 in the solution (Fig. 6). Apparently, the deposited $FeCO_3$ layer on electrode surface formed in the CO_2-containing solution cannot provide effective inhibition to crack initiation. The enhanced fracture brittleness is attributed to the evolution and penetration of hydrogen atoms into the steel, which contribute to crack propagation. Therefore, the deposit layer is not effective in reducing hydrogen permeation either, which is mainly due to the loose, porous structure of the film. Hydrogen atoms generated from the cathodic reduction of carbonate acid can enter directly into steel from the pores in the deposit, rather than diffuse through the deposit layer.

5. Conclusions

The electrochemical corrosion of X70 steel in aerated, alkaline solution is an activation-controlled process, and a stable passive region was not observed for the steel.

Corrosion rate of the steel increases with the CO_2 partial pressure. The enhanced anodic dissolution due to the additional cathodic reaction in the presence of CO_2, rather than the film-formation reaction, dominates the corrosion process. The mass-transfer step through $FeCO_3$ deposit is the rate-controlling step in corrosion of the steel.

The susceptibility of steel to SCC and the fracture brittleness increase with the CO_2 partial pressure. The enhanced fracture brittleness is attributed to the evolution and penetration of hydrogen atoms into the steel, and contributes to crack propagation. The deposit layer is not effective in reducing hydrogen permeation due to its loose, porous structure.

Acknowledgments

This work was supported by Chinese National Science and Technology Infrastructure Platforms Construction Projects (No. 2005DKA 10400) and National Science and Technology Support—The 11th Five-Year Plan (2006BAK02B01).

References

1. S. Nesic, Key Issues Related to Modeling of Internal Corrosion of Oil and Gas Pipelines—A Review, *Corros. Sci.*, 2007, **49**, p 4308–4338
2. C. de Waard, U. Lotz, and D.E. Milliams, Predictive Model for CO_2 Corrosion Engineering in Wet Natural Gas Pipelines, *Corrosion*, 1991, **31**, p 976–985
3. S. Turgoose, R.A. Cottis, and K. Lawson, *Modelling of Electrode Processes and Surface Chemistry in Carbon Dioxide Containing Solution*, ASTM Symposium on Computer Modelling of Corrosion, San Antonio, 1990
4. S. Nesic, J. Postlethwaite, and S. Olsen, An Electrochemical Model for Prediction of Corrosion of Mild Steel in Aqueous Carbon Dioxide Solutions, *Corrosion*, 1996, **52**, p 280–294
5. R.N. Parkins and S. Zhou, The Stress Corrosion Cracking of C-Mn Steel in CO_2–HCO_3^-–CO_3^{2-} Solutions. I: Stress Corrosion Data, *Corros. Sci.*, 1997, **39**, p 159–173
6. R.N. Parkins and S. Zhou, The Stress Corrosion Cracking of C-Mn Steel in CO_2–HCO_3^-–CO_3^{2-} Solutions. II: Electrochemical and Other Data, *Corros. Sci.*, 1997, **39**, p 175–191
7. R.N. Parkins, A Review of Stress Corrosion Cracking of High. Pressure Gas Pipelines, Corrosion/2000, Paper no. 363. NACE, Houston, 2000
8. R.L. Eadie, K.E. Szklarz, and R.L. Sutherby, Corrosion Fatigue and Near-Neutral pH Stress Corrosion Cracking of Pipeline Steel and the Effect of Hydrogen Sulfide, *Corrosion*, 2005, **61**, p 167–173
9. L. Niu and Y.F. Cheng, Corrosion Behavior of X-70 Pipe Steel in Near-Neutral pH Solution, *Appl. Surf. Sci.*, 2007, **253**, p 8626–8631
10. M.C. Li and Y.F. Cheng, Mechanistic Investigation of Hydrogen-Enhanced Anodic Dissolution of X-70 Pipe Steel and Its Implication on Near-Neutral pH SCC of Pipelines, *Electrochimica Acta*, 2007, **52**, p 8111–8117
11. Y.F. Cheng and J.L. Luo, Passivity and Pitting of Carbon Steel in Chromate Solutions, *Electrochimica Acta*, 1999, **44**, p 4795–4804
12. B.R. Tian and Y.F. Cheng, Electrochemical Corrosion Behavior of X-65 Steel in the Simulated Oil Sand Slurry. I: Effects of Hydrodynamic Condition, *Corros. Sci.*, 2008, **50**, p 773–779
13. S. Nesic, M. Nordsveen, R. Nyborg, and A. Stangeland, A Mechanistic Model for CO2 Corrosion with Protective Iron Carbonate Films, Corrosion/2001, Paper no. 01040, NACE, Houston, 2001
14. Y.F. Cheng, Corrosion of X-65 Pipeline Steel in Carbon Dioxide-Containing Solutions, *Bull. Electrochem.*, 2005, **21**, p 503–511